A Simple and Effective Method for Removing Residual Reflected Skylight in Above-water Remote Sensing Reflectance Measurements

Dalin Jiang[1], Bunkei Matsushita[2*], Wei Yang[3]

1. Graduate School of Life and Environmental Sciences, University of Tsukuba, Tsukuba, Ibaraki 305-8572, Japan
2. Faculty of Life and Environmental Sciences, University of Tsukuba, Tsukuba, Ibaraki 305-8572, Japan
3. Center for Environmental Remote Sensing, Chiba University, Chiba 263-8522, Japan

Submittal date: March 2, 2020

*Corresponding Author

Phone: 81-29-853-7190

Fax: 81-29-853-7190

Email: matsushita.bunkei.gn@u.tsukuba.ac.jp

A Simple and Effective Method for Removing Residual Reflected Skylight in Above-water Remote Sensing Reflectance Measurements

Abstract: In situ remote sensing reflectance (R_{rs}) measured using the above-water approach usually suffers from residual reflected skylight (Δ), and thus its applicability is limited. In this study, we proposed a simple method, which only required the in situ R_{rs} spectrum itself as input, to further remove the Δ effects in the in situ R_{rs} spectrum. The performance of the proposed method was evaluated using both simulation data and in situ R_{rs} spectra measured using a radiance sensor with a black tube (Δ-free in situ R_{rs}). The results showed that the proposed method outperformed other existing methods and can be applied to various types of waters. For example, from the two simulation experiments, it was seen that the proposed method can provide accurate R_{rs} spectra with a mean absolute percentage error (MAPE)=6% even if they are measured under various sky conditions and wind speeds (using Hydrolight) and can estimate accurate Δ values with MAPE=5% (using a simple bio-optical model). From a comparison analysis using Δ-free in situ R_{rs} data, the proposed method also showed the best performance with the smallest MAPE of 45% (MAPE ranged from 52% to 260% for other existing methods). In addition, the proposed method can improve the quality of R_{rs} spectra collected under various sky conditions (clear, scattered clouds and overcast), with an increased proportion of higher quality assurance scores. Two showcases indicate that the Δ corrections should be carried out for all above water approach-measured R_{rs} spectra before they are applied to develop water quality estimation algorithms or to evaluate the performances of atmospheric correction algorithms.

Keywords: above-water approach, residual reflected skylight, water absorption at 810 nm, various waters

1 Introduction

Remote sensing reflectance (R_{rs}) is defined as the ratio of water-leaving radiance ($L_w(\lambda)$) and downwelling irradiance ($E_d(\lambda)$) just above the water surface (Kirk, 2011). It is an important parameter in ocean (water) color remote sensing, which is always required to develop estimation algorithms of water quality parameters and to evaluate the performances of the developed atmospheric correction algorithms (Wang et al., 2009; Guanter et al., 2010; Goyens et al., 2013; Jaelani et al., 2013; Wei et al., 2016; Cao et al., 2018; Jiang et al., 2019).

Compared to the in-water approach, the above-water approach is relatively easy to implement in a field survey, and thus is widely used to collect R_{rs} data (Mueller et al., 2000; Zibordi et al., 2012). However, the $L_w(\lambda)$ cannot be directly measured due to the specular reflections on the water surface caused by diffuse solar irradiance (i.e., surface-reflected radiance), which are picked-up simultaneously by this method. To solve this problem, measuring the radiance of skylight ($L_s(\lambda)$) has been suggested, and R_{rs} is calculated using the following equation (Mobley, 1999):

$$R_{rs}(\lambda) = \left(L_t(\lambda) - \rho L_s(\lambda)\right) / \left(\frac{\pi}{R_g(\lambda)} L_g(\lambda)\right) , \quad (1)$$

where $L_t(\lambda)$ is the total upwelling radiance from the water and can be directly measured by a sensor; ρ is the skylight reflectance and is equal to 0.028 when the wind speed is less than 5 m/s; $L_g(\lambda)$ is the upwelling radiance from a standard gray board; and $R_g(\lambda)$ is the reflectance of the gray board.

Since it is very difficult to determine an accurate ρ value under different conditions of light, wind and viewing geometry, many researchers have suggested that further removal of residual reflected skylight (hereafter Δ) is necessary to obtain more accurate R_{rs} spectra (Ruddick et al., 2005; Lee et al., 2010; Kutser et al., 2013; Groetsch et al., 2017; Bernardo et al., 2018), e.g.:

$$R_{rs}(\lambda) = \left(L_t(\lambda) - \rho L_s(\lambda)\right) / \left(\frac{\pi}{R_g(\lambda)} L_g(\lambda)\right) - \Delta \ . \quad (2)$$

Currently, there are three types of approaches for removing Δ. The first type involves assuming

74 Δ to be equal to the R_{rs} value at near-infrared (for clear waters) or middle-infrared (for turbid waters)
75 wavelengths because the R_{rs} values at these wavelengths can be assumed to be zero due to the strong
76 absorption of pure water and the weak backscatters of suspended particles (i.e., dark pixel
77 assumption) (e.g., Choi et al., 2012, 2014; Qiu, 2013; Zhang et al., 2010; Cai et al., 2015; Dierssen et
78 al., 2006; Brewin et al., 2016; Froidefond et al., 2002; Knaeps et al., 2012; Song et al., 2012). However,
79 since the wavelength of the dark pixel assumption will change in different water types, it is difficult
80 to objectively determine an appropriate wavelength.

81 The second type of approach is estimating Δ based on various assumptions (e.g., Ruddick et
82 al., 2005, 2006; Lee et al., 2010; Dev and Shanmugam, 2014). For example, Ruddick et al. (2005,
83 2006) found that the spectral shape in the near-infrared domain (700–900 nm) is almost invariant,
84 and thus they proposed a similarity spectrum method under the assumption of a fixed ratio of $R_{rs}(720)$
85 and $R_{rs}(780)$ (i.e., $R_{rs}(720)/R_{rs}(780)=2.35$). However, as pointed out in Ruddick et al. (2005), the
86 applicability of this method is limited to medium turbid waters with $R_{rs}(720) \leq 0.0095$ sr^{-1}
87 (corresponding to water-leaving irradiance reflectance of 0.03 in Ruddick et al., 2005). Lee et al.
88 (2010) proposed an optimization method to estimate Δ. They first simulated the R_{rs} as the magnitude
89 of the absorption coefficient of phytoplankton, gelbstoff and the backscattering coefficient of
90 particles, and then solved for Δ by matching the simulated R_{rs} with the in situ-measured R_{rs} spectra.
91 However, since the method requires the specific inherent optical properties (SIOPs) of each optical
92 active matter in a water body to generate synthetic R_{rs} spectra, it can be considered that a larger error
93 will occur if the method is applied to a water body with different SIOPs. In addition, the wavelength
94 ranges used for optimization should be changed according to the turbidity of a water body (Lee et
95 al., 2010).

96 The third type of approach involves directly estimating the surface-reflected radiance rather
97 than estimating Δ (Kutser et al., 2013; Groetsch et al., 2017). Kutser et al. (2013) found that the
98 surface-reflected radiance can be obtained by fitting the spectral ranges of 350–380 nm and 890–

900 nm using a power function. However, this finding is only suitable for colored dissolved organic matter (CDOM)-rich waters (Kutser et al., 2013). Groetsch et al. (2017) proposed to apply a three-component reflectance model (3C) to above-water radiometric measurements for estimating surface-reflected radiance. Similar to the method of Lee et al. (2010), the 3C-based method also needs SIOPs to generate synthetic L_t spectra for optimization, and thus has limitations in its application to waters with different SIOPs.

Consequently, the objectives of this research are to: (1) develop a new method for removing the residual reflected skylight (Δ) in above-water R_{rs} measurements that can overcome the above shortcomings in the existing methods; (2) evaluate the performance of the proposed method by comparing it with four existing methods using both simulated and in situ collected data; (3) provide showcases to further confirm significances of Δ–correction.

2 Data collection

2.1 In situ data collection

In situ R_{rs} spectra and corresponding Secchi disk depth (Z_{SD}) data were collected from field surveys in 21 Japanese inland waters during 2009 and 2019 and the SeaWiFS Bio-optical Archive and Storage System (SeaBASS) database.

The 21 Japanese inland waters include 20 lakes and 1 bay (Tokyo Bay; Fig. 1a), with Z_{SD} values ranging from 0.3 m to 16.4 m, chlorophyll-a (Chl-a) concentrations ranging from 0.5 mg/m^3 to 187.7 mg/m^3, and total suspended solids (TSS) concentrations ranging from 0.4 g/m^3 to 73.7 g/m^3 (Table 1). For each site, the radiance of the skylight (L_s), the radiance from a standard gray board (L_g), and the total upwelling radiance from the water (L_t) were measured using a FieldSpec® HandHeld spectroradiometer (ASD Inc., Boulder, CO) with a sensor zenith angle (θ) of 40° and an azimuth angle (ϕ) of 135° (Mobley, 1999; Mueller et al., 2000). The R_{rs} was then calculated using Eq. (1) with the skylight reflectance ρ=0.028 (when the wind speed was < 5 m/s, Mobley, 1999). Z_{SD} was

124 measured by lowering a 30 cm diameter white disk into the water until the disk was no longer visible
125 (Wernand, 2010; Aas et al., 2014). We kept all R_{rs} spectra collected under different sky conditions
126 (i.e., clear, scattered clouds, and overcast). These sky conditions were distinguished using the
127 method of Groetsch et al. (2017). In total, 305 pairs of in situ R_{rs} spectra and corresponding Z_{SD}
128 values were obtained from Japanese inland waters.

129 Moreover, three experiments were carried out in two Japanese lakes (Lake Kasumigaura with
130 Z_{SD}=0.8 m on March 12, 2019 and Lake Chuzenji with Z_{SD}=9.7 m on June 4, 2019) and one
131 Indonesian lake (Lake Tamblingan with Z_{SD}=2.1 m on March 20, 2019). Except for in situ R_{rs} spectra
132 measured using the above-water approach, three Δ-free R_{rs} spectra were also measured using
133 RAMSES spectroradiometer (TriOS, Rastede, Germany). Since a black tube (5 cm) was installed in
134 front of the downward radiance sensor and kept just below water surface, L_w was directly measured
135 without Δ effects (Lee et al., 2010; Kutser et al., 2013). At the same time, E_d just above the water
136 surface was measured using an upward irradiance sensor. All R_{rs} spectra were measured under clear
137 sky condition with wind speed lower than 5 m/s.

138 For the SeaBASS database, we only chose the R_{rs} spectra with wavelengths ranging from 400
139 nm to 850 nm and the corresponding Z_{SD} values. As a result, a total of 167 data pairs were obtained.
140 These data pairs were collected from San Francisco Bay, the northern Gulf of Mexico, Chesapeake
141 Bay, and Lake Erie (Fig. 1b). The Δ corrections had already been carried out by the providers for
142 some of the selected in situ R_{rs} spectra. The Z_{SD} values of the selected data pairs ranged from 0.2 m
143 to 45 m.
144

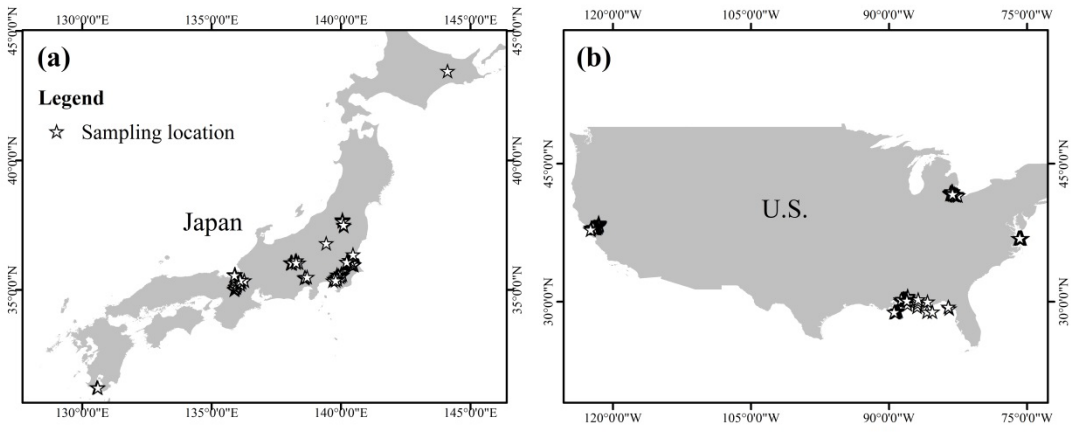

146 Fig. 1. Locations of in situ data used in this study. (a) Data collected from 21 Japanese inland waters;

147 (b) data collected from SeaBASS.

148

149 Table 1. Name, area, Z_{SD}, Chl-a, TSS, and number of data of the 21 Japanese inland waters.

Name	Area (km^2)	Z_{SD} (m)	Chl-a (mg/m^3)	TSS (g/m^3)	Number of data	Sampling year
Biwa	670.3	2.3-10.7	0.6-7.0	0.6-3.4	58	2009-2011
Kasumigaura	167.6	0.3-1.2	12.0-187.7	4.1-73.7	181	2009-2019
Inawashino	103.3	9.3-10	0.6-0.7	1.0-1.1	2	2010
Akan	13.0	6.7	0.8	1.5	1	2013
Suwa	12.9	0.9-1.9	9.8-29.4	4.4-9.6	21	2010-2018
Ikeda	10.9	9.3	1.4	0.7	1	2011
Hibara	10.7	6.1-7.3	1.7-2.3	1.0-1.3	4	2018
Motosu	4.7	9.3-16.4	0.6	0.4	2	2014
Suigetsu	4.2	1.0-1.5	3.9	3.6	2	2016
Mikata	3.6	0.8	6.3	8.0	1	2016
Sai	2.1	6.8-7.1	1.8	1.3	2	2014
Kugushi	1.4	1.4	27.4	5.9	1	2016
Unagi	1.2	12.8	0.5	0.4	1	2011

Suga	0.9	0.8	57.0	7.5	1	2016
Shoji	0.5	3.5-4.2	3.2-8.5	1.7-2.4	2	2014
Shirakaba	0.4	1.0-3.5	2.3-26.9	2.8-9.1	3	2010-2018
Senbako	0.33	0.6	98.9	29.2	1	2019
Yunoko	0.32	3.4	4.5	1.9	1	2011
Megami	0.12	2.4	5.7	3.8	1	2018
Tateshina	0.08	2.5	6.5	3.1	1	2018
Tokyo Bay	1500	1.9-5.5	2.9-32.0	2.1-4.3	18	2010-2011
Total	--	0.3-16.4	0.5-187.7	0.4-73.7	305	2009-2019

2.2 Generating synthetic data

As it is very difficult to measure an error-free R_{rs} spectrum in the field, we used a bio-optical model to obtain error-free R_{rs} spectra. The bio-optical model can be expressed as follows (Gordon et al., 1988; Lee et al., 2002):

$$R_{rs}(\lambda) = \frac{0.52 r_{rs}(\lambda)}{1 - 1.7 r_{rs}(\lambda)} \quad (3)$$

$$r_{rs}(\lambda) = 0.089\left(\frac{b_b(\lambda)}{a(\lambda)+b_b(\lambda)}\right) + 0.125\left(\frac{b_b(\lambda)}{a(\lambda)+b_b(\lambda)}\right)^2 , \quad (4)$$

where $r_{rs}(\lambda)$ is the remote sensing reflectance just below the water surface, $a(\lambda)$ is the total absorption coefficient of water, and $b_b(\lambda)$ is the total backscattering coefficient of water. The $a(\lambda)$ and $b_b(\lambda)$ can be further separated as follows (Vahtmäe et al., 2006; Yang et al., 2011):

$$a(\lambda) = C_{chl} \cdot a^*_{ph}(\lambda) + C_{tr} \cdot a^*_{tr}(\lambda) + C_{CDOM} \cdot a^*_{CDOM}(\lambda) + a_w(\lambda) \quad (5)$$

$$b_b(\lambda) = C_{chl} \cdot b^*_{bph}(\lambda) + C_{tr} \cdot b^*_{btr}(\lambda) + b_{bw}(\lambda) , \quad (6)$$

where C_{chl} is the concentration of Chl-a, C_{tr} is the concentration of tripton, and C_{CDOM} is the absorption coefficient of CDOM at 440 nm. The parameters $a^*_{ph}(\lambda)$, $a^*_{tr}(\lambda)$, and $a^*_{CDOM}(\lambda)$ are the specific absorption coefficients of phytoplankton, tripton, and CDOM, respectively. $b^*_{bph}(\lambda)$ and $b^*_{btr}(\lambda)$ are the specific backscattering coefficients of phytoplankton and tripton, respectively. $a_w(\lambda)$

166 is the absorption coefficient of pure water (Kou et al., 1993; Pope and Fry, 1997; Lee et al., 2015a),

167 and $b_{bw}(\lambda)$ is the backscattering coefficient of pure water (Zhang et al., 2009).

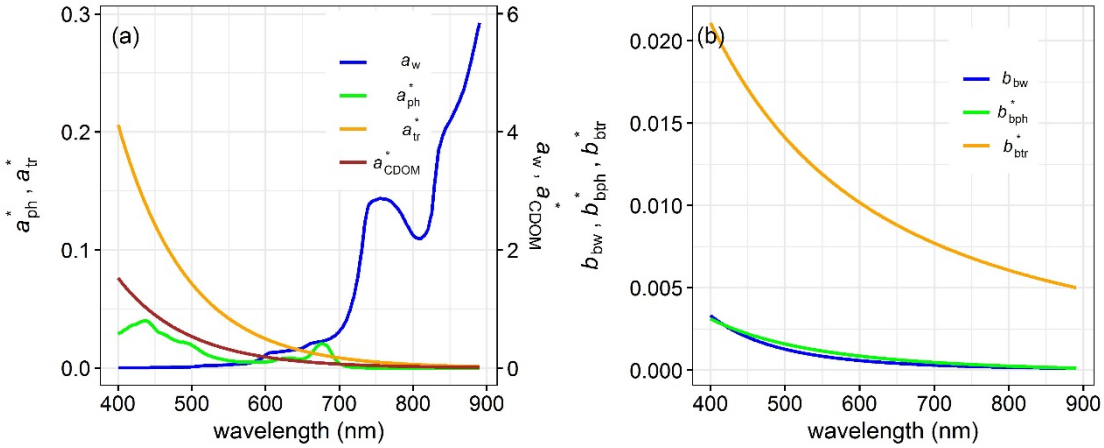

169 Fig. 2. Specific inherent optical properties (SIOPs) collected from Lake Kasumigaura, Japan, on

170 May 11, 2018. (a) a_w (m^{-1}) is the absorption coefficient of pure water, a^*_{ph} (m^2/mg), a^*_{tr} (m^2/g), and

171 a^*_{CDOM} (dimensionless) are the specific absorption coefficients of phytoplankton, tripton, and

172 CDOM, respectively; (b) b_{bw} (m^{-1}) is the backscattering coefficient of pure water; and b^*_{bph} (m^2/mg)

173 and b^*_{btr} (m^2/g) are the specific backscattering coefficients of phytoplankton and tripton, respectively.

174

175 We generated two synthetic datasets using the above bio-optical model (hereafter Synthetic

176 Dataset I and Synthetic Dataset III), and another synthetic dataset using Hydrolight (Mobley, 1994;

177 hereafter Synthetic Dataset II). Dataset I was used to develop a method for Δ correction, and Dataset

178 II and Dataset III were used to evaluate the performance of the developed method.

179 Synthetic Dataset I was generated for various water turbidities. The concentrations of Chl-a

180 and tripton were varied between 0.01 mg/m^3 and 300 mg/m^3 and between 0.01 g/m^3 and 300 g/m^3,

181 respectively. The absorption coefficient of CDOM at 440 nm was varied between 0.01 m^{-1} and 10

182 m^{-1}. The intervals of the Chl-a (tripton) concentration were 0.01 mg/m^3 (g/m^3) for 0.01–0.1 mg/m^3

183 (g/m^3), 0.1 mg/m^3 (g/m^3) for 0.1–1.0 mg/m^3 (g/m^3), 1.0 mg/m^3 (g/m^3) for 1.0–10 mg/m^3 (g/m^3), 2

184 mg/m^3 (g/m^3) for 10–20 mg/m^3 (g/m^3), 5 mg/m^3 (g/m^3) for 20–50 mg/m^3 (g/m^3), 10 mg/m^3 (g/m^3)

for 50–100 mg/m^3, and 20 mg/m^3(g/m^3) for 100–300 mg/m^3(g/m^3). For CDOM, the intervals were 0.01 m^{-1} for 0.01–0.1 m^{-1}, 0.1 m^{-1} for 0.1–1.0 m^{-1}, 1.0 m^{-1} for 1.0–5 m^{-1}, and 2 m^{-1} for 5–10 m^{-1}. The SIOPs were collected from Lake Kasumigaura on May 11, 2018 (Fig. 2). In total, 75816 error-free R_{rs} spectra were generated. Figure 3 shows 200 randomly selected examples of simulated R_{rs} spectra.

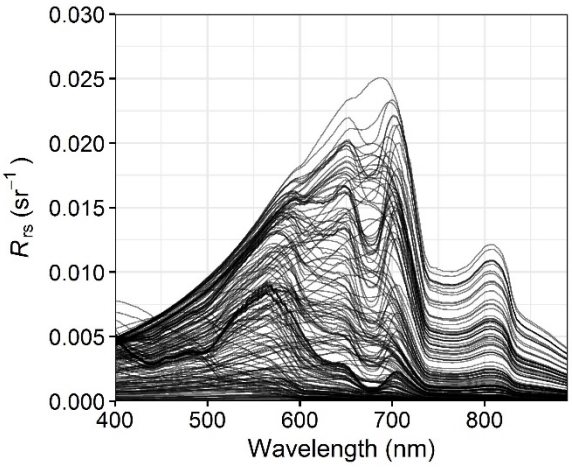

Fig. 3. 200 randomly selected R_{rs} spectra from Synthetic Dataset I.

Synthetic Dataset II was generated using the Hydrolight radiative transfer model (version 5, Sequoia Scientific), which can solve the radiative transfer equation to compute the radiance distribution within and leaving a water body. The Hydrolight provides default SIOPs for four components (pure water, Chl-a, mineral particles, and CDOM), which were directly used in this study. The water was assumed to be homogeneous and of infinite depth. Raman scattering was ignored in this simulation. The refraction index was set as 1.34, and the sun zenith angle was kept at 30 degrees. The semi-empirical sky-model based on RADTRAN was used to simulate the solar and sky irradiance incident onto the water surface. The Chl-a concentration was set as 35 mg/m^3, the mineral particles concentration was set as 15 g/m^3, and the CDOM absorption coefficient at 440 nm was set as 0.8 m^{-1}.

To simulate various environmental conditions that we may face in the field, we ran the Hydrolight by combining different wind speeds, cloud cover percentages, and view geometries

(Table 2). In total, we simulated 12 cases and obtained the corresponding L_t, $L_{s,}$ and E_d spectra between 350–900 nm with a 5 nm interval. The R_{rs} spectrum simulated under the conditions of a clear sky, wind speed=0 m/s, and the recommended view geometry (θ=40°, ϕ=135°) was considered to be Δ-free R_{rs} (i.e., Case 1 in Table 2). The other 11 R_{rs} spectra calculated from the simulated L_t, $L_{s,}$ and E_d spectra by Eq. (1) were considered to be Δ-contaminated R_{rs} and were used to evaluate the proposed Δ correction method.

Table 2. Conditions of radiative transfer simulation for generating Synthetic Dataset II.

Case	Wind speed (m/s)	Cloud cover (%)	View geometry(θ,ϕ)
1 (Δ-free)	0	0 (clear sky)	(40°, 135°)
2 (with Δ effects)	0	50 (scattered clouds)	(40°, 135°)
3 (with Δ effects)	0	100 (overcast)	(40°, 135°)
4 (with Δ effects)	10	0 (clear sky)	(40°, 135°)
5 (with Δ effects)	10	50 (scattered clouds)	(40°, 135°)
6 (with Δ effects)	10	100 (overcast)	(40°, 135°)
7 (with Δ effects)	0	0 (clear sky)	(50°, 90°)
8 (with Δ effects)	0	50 (scattered clouds)	(50°, 90°)
9 (with Δ effects)	0	100 (overcast)	(50°, 90°)
10 (with Δ effects)	10	0 (clear sky)	(50°, 90°)
11 (with Δ effects)	10	50 (scattered clouds)	(50°, 90°)
12 (with Δ effects)	10	100 (overcast)	(50°, 90°)

For Synthetic Dataset III, we first randomly selected 1000 Chl-a concentrations in the range of 0.01–300 mg/m^3, 1000 tripton concentrations in the range of 0.01–300 g/m^3, and 1000 absorption coefficients of CDOM at 440 nm in the range of 0.01–10 m^{-1}, to generate 1000 error-free R_{rs} spectra

using the same bio-optical model described above. Secondly, we randomly generated 1000 Δ values in the range of 0 sr^{-1} to 0.01 sr^{-1} (true Δ) and added them to each error-free R_{rs} spectra to generate 1000 Δ-contaminated R_{rs} spectra. Synthetic Dataset III was used to evaluate the performance of the proposed method by comparing the estimated Δ values using the proposed method with the true Δ values.

2.3 Accuracy assessment

We mainly used the root mean square error (RMSE), the mean absolute percentage error (MAPE), and bias to evaluate the performance of the proposed method. The equations are as follows:

$$\mathrm{RMSE} = \sqrt{\frac{\sum_{i=1}^{N}\left(X_{\mathrm{estimated},i} - X_{\mathrm{measured},i}\right)^2}{N}} \quad (7)$$

$$\mathrm{MAPE} = \frac{1}{N}\sum_{i=1}^{N}\left|\frac{X_{\mathrm{estimated},i} - X_{\mathrm{measured},i}}{X_{\mathrm{measured},i}}\right| \cdot 100\% \quad (8)$$

$$\mathrm{Bias} = \frac{1}{N}\sum_{i=1}^{N}\left(X_{\mathrm{estimated},i} - X_{\mathrm{measured},i}\right) , \quad (9)$$

where $X_{\mathrm{estimated}}$ is the estimated parameter (e.g., R_{rs}, Δ or Z_{SD}), X_{measured} is the corresponding in situ measurement (or true value), and N is the number of data pairs. The regression results between estimated and in situ-measured parameters were also used for assistance (e.g., slope, intercept, and R^2).

In addition, a spectral quality assessment system proposed by Wei et al. (2016) was also used to calculate quality assurance (QA) scores for the R_{rs} spectra before and after Δ corrections. The QA scores can vary from 0/9 (which means that none of the 9 tested wavelengths can be used, i.e., unusable R_{rs} spectra) to 9/9 (which means that all 9 tested wavelengths are useful, i.e., perfect R_{rs} spectra).

The performances of the four existing methods for Δ correction were also evaluated using the above indices and compared to the new method. The four existing methods were proposed by Ruddick et al. (2005, hereafter R05), Lee et al. (2010, hereafter L10), Kutser et al. (2013, hereafter K13), and Groetsch et al. (2017, hereafter G17), respectively. Note that the K13 method and G17

method were only applied to R_{rs} spectra collected in Japan and Indonesia, as these two methods require L_s, L_t, and E_d as inputs, which are not available from the SeaBASS database. In addition, we refer to the method proposed by Mobley (1999, i.e. Eq. (1)) with a fixed ρ value of 0.028 as "M99" in this study.

3 A new method for Δ correction

3.1 Finding an index without Δ effect

Residual reflected skylight (i.e., Δ), such as an error due to an imperfect atmospheric correction, is a kind of noise from the light environment in addition to the R_{rs} spectrum. Therefore, the Δ effect can be minimized/removed using baseline-based indices such as FLH (Fluorescence Line Height), MCI (Maximum Chlorophyll-a Index), CI (Color Index) and so on, if we assume the Δ is a wavelength-independent variable (e.g., Gower 1980; Gower et al., 2005; Hu et al., 2012; Matsushita et al., 2016).

On the other hand, to make a baseline-based index that can be applied to various waters, it is desirable that the index be insensitive to the variation of water SIOPs. From Fig. 2, it can be seen that the SIOPs in the near-infrared domain are only dominated by the absorption coefficient of pure water. Therefore, a baseline-based index using near-infrared wavelengths can meet this requirement.

According to the above considerations, we noticed that the relative height of the water-absorption-dip-induced-reflectance-peak-at-810 nm (hereafter RHW; Figs. 2 and 3) can meet both requirements. The RHW can be calculated using the following equations:

$$\mathrm{RHW} = R_{rs}(810) - R'_{rs}(810) \tag{10}$$

$$R'_{rs}(810) = R_{rs}(780) + \left(R_{rs}(840) - R_{rs}(780)\right) \times (810 - 780)/(840 - 780), \tag{11}$$

where $R_{rs}(780)$, $R_{rs}(810)$, and $R_{rs}(840)$ are the remote sensing reflectance at 780 nm, 810 nm, and 840 nm measured from above the water surface, respectively.

3.2 Estimating Δ-free R_{rs}(810) from RHW

Previous studies have confirmed that there exists a strong correlation between the concentration of TSS and R_{rs} values in the near-infrared domain (e.g., Nechad et al., 2010; Yang et al., 2011). Therefore, TSS can be expressed as follows using R_{rs} values in the near-infrared domain. For example:

$$TSS=f_1(R_{rs}(780))=f_2(R_{rs}(810))=f_3(R_{rs}(840)) \quad (12)$$

where f_1-f_3 represent functions to obtain TSS from R_{rs}(780), R_{rs}(810) and R_{rs}(840), respectively. From Eq. (12), it can be deduced that there is a correlation between the R_{rs} values at the above three near-infrared wavelengths. In addition, since the RHW is calculated from R_{rs}(780), R_{rs}(810) and R_{rs}(840), we can obtain the following equation:

$$R_{rs}(810)=f_4(\mathrm{RHW}), \quad (13)$$

where f_4 represents a function to obtain R_{rs}(810) from RHW. Eq. (13) indicates that we can obtain Δ-free R_{rs}(810) even when using R_{rs} spectra with Δ effects if a relationship between Δ-free R_{rs}(810) and RHW was constructed. The R_{rs}(810) was selected is because that it locates at a reflectance peak and thus has higher signal-to-noise ratio (SNR) comparing to R_{rs}(780) and R_{rs}(840).

To construct the relationship between Δ-free R_{rs}(810) and RHW, we used Synthetic Dataset I (N = 75816). Figure 4 shows the relationship between R_{rs}(810) and RHW. It can be seen that there certainly exists a very good nonlinear relationship between the two variables. The nonlinear relationship is as follows:

$$R_{rs}(810) = 16865.541\mathrm{RHW}^3 - 52.728\mathrm{RHW}^2 + 3.361\mathrm{RHW} \quad (14)$$

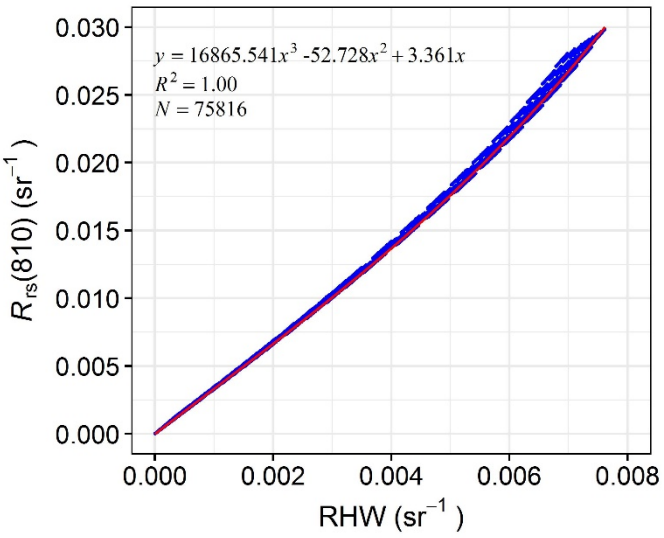

287 Fig. 4. Relationship between $R_{rs}(810)$ and RHW obtained from Synthetic Dataset I.

288

289 3.3 Estimating and removing Δ effects

290 First, we can calculate the R_{rs} from the measured L_s, L_t, and L_g using Eq. (1), and obtain the R_{rs}

291 value at 810 nm (hereafter referred to as measured-$R_{rs}(810)$). Clearly, the measured-$R_{rs}(810)$ value

292 contains an Δ effect. Then, based on the assumption of a wavelength independent of Δ, it can be

293 considered that we can estimate Δ-free $R_{rs}(810)$ using Eq. (14) even if we use an R_{rs} spectrum with

294 an Δ effect (hereafter referred to as estimated-$R_{rs}(810)$). Finally, we can estimate Δ by taking the

295 difference between measured-$R_{rs}(810)$ and estimated-$R_{rs}(810)$.

296 Practically speaking, to further reduce the noise effects on in situ-measured R_{rs} spectra, the

297 implementation of a Savitzky–Golay filter with a 21 nm window is recommended after calculating

298 R_{rs} spectra using Eq. (1). The flowchart for Δ correction is shown in Fig. 5.

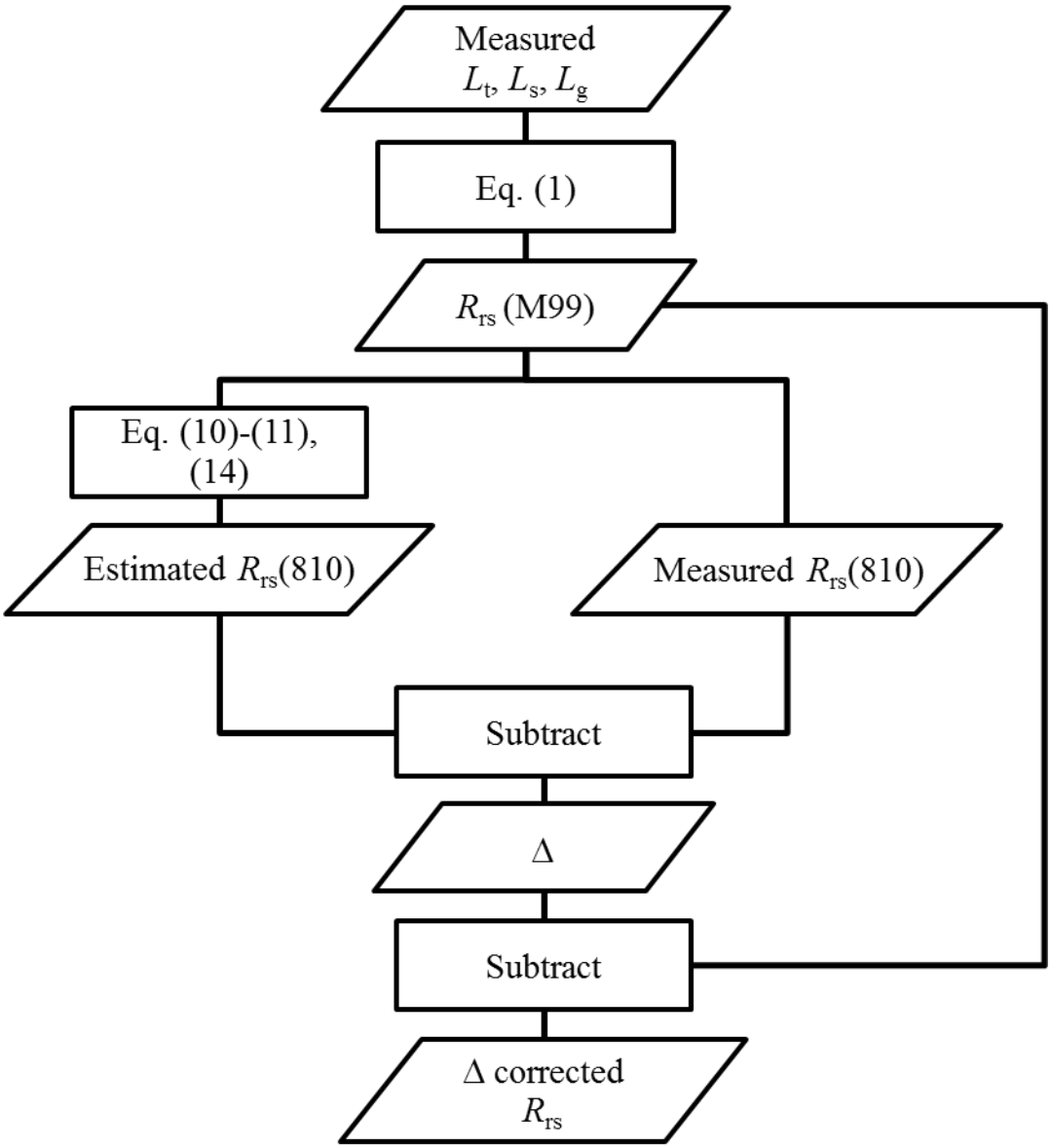

300 Fig. 5. Flowchart of the proposed method for Δ correction. R_{rs}(M99) represents the remote sensing
301 reflectance calculated using Eq. (1) with a constant ρ value of 0.028 (Mobley, 1999).
302
303 4 Performance of the new method
304 4.1 Evaluation using in situ-measured Δ-free R_{rs} spectra as well as Synthetic Datasets II and III
305 Figure 6 shows the comparisons of above-water R_{rs} measurements corrected by different
306 methods (solid lines) and corresponding in situ-measured Δ-free R_{rs} spectra (dashed lines) in two
307 Japanese lakes and one Indonesian lake. It can be seen that: (1) overall, the method proposed in this
308 study showed the best performance with the smallest RMSE (0.00047 sr^{-1}), MAPE (45%), and bias

(0.00014 sr^{-1}), but also with noticeable inconsistencies at wavelengths shorter than 450 nm in the two Japanese lakes (red and blue lines in Fig. 6f); (2) the K13 method failed in correcting all above-water R_{rs} measurements with the largest error indices (Fig. 6b); (3) the G17 method and the L10 method mainly showed worse performance than the proposed method in this study in Lake Kasumigaura (red lines in Fig. 6c) and Lake Tamblingan (green lines in Fig. 6d), respectively; and (4) comparing to the method proposed in this study, the R05 method had lower accuracy in Lake Kasumigaura and similar accuracies in the other two lakes (Fig. 6e).

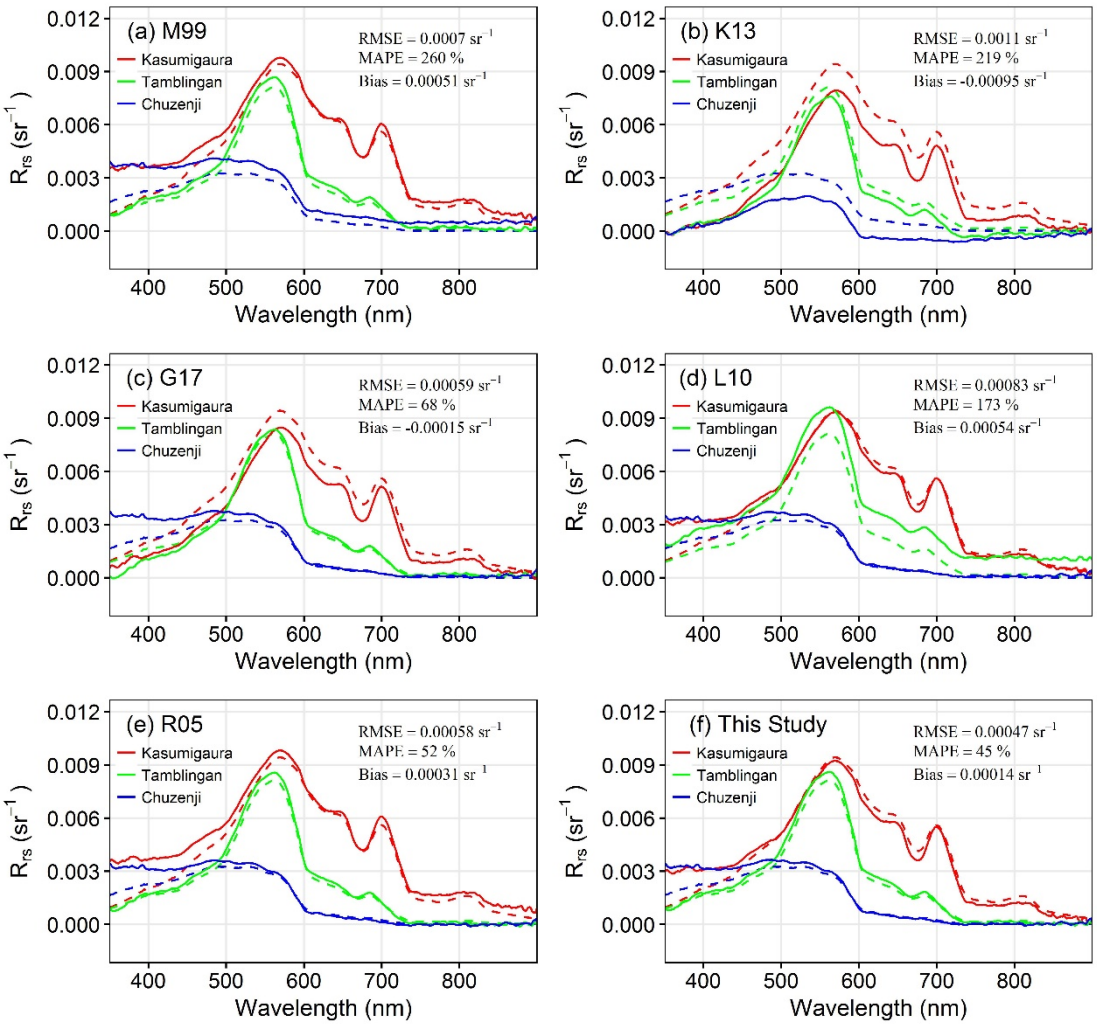

Fig. 6. Comparison of above-water R_{rs} measurements corrected by different methods (solid lines) and corresponding in situ-measured Δ-free R_{rs} spectra (dashed lines) in two Japanese lakes (Lake Kasumigaura with Z_{SD}=0.8 m, and Lake Chuzenji with Z_{SD}=9.7 m) and one Indonesian lake (Lake

Tamblingan with Z_{SD}=2.1 m). (a) using the M99 method (without Δ correction); (b) using the K13 method; (c) using the G17 method; (d) using the L10 method; (e) using the R05 method; (f) using the new method proposed in this study.

As it is really not easy to obtain a large number of Δ-free R_{rs} spectra from the field surveys, we also used synthetic data to further evaluate the performance of the new method. Figure 7 shows the comparisons of Δ-corrected R_{rs} spectra (blue lines) and the true R_{rs} spectrum (red line) using Synthetic Dataset II. It can be seen that the R_{rs} spectra estimated using the M99 method exhibited substantial variation at all wavelengths, even though they had the same IOPs (Fig. 7a). This variation was reduced after Δ corrections were carried out (Figs. 7b-7f). The method proposed in this study performed well at all wavelengths with the smallest RMSE (0.00043 sr^{-1}) and MAPE (6%), followed by the G17 method (RMSE=0.00059 sr^{-1}, MAPE=11%, overcorrections at shorter wavelengths), R05 method (RMSE=0.00066 sr^{-1}, MAPE=19%, overcorrections at both shorter and longer wavelengths), and L10 method (RMSE=0.00099 sr^{-1}, MAPE=20%, under corrections at all wavelengths). The K13 method overcorrected the Δ effects at all wavelengths with a large RMSE (0.0016 sr^{-1}) and MAPE (39%).

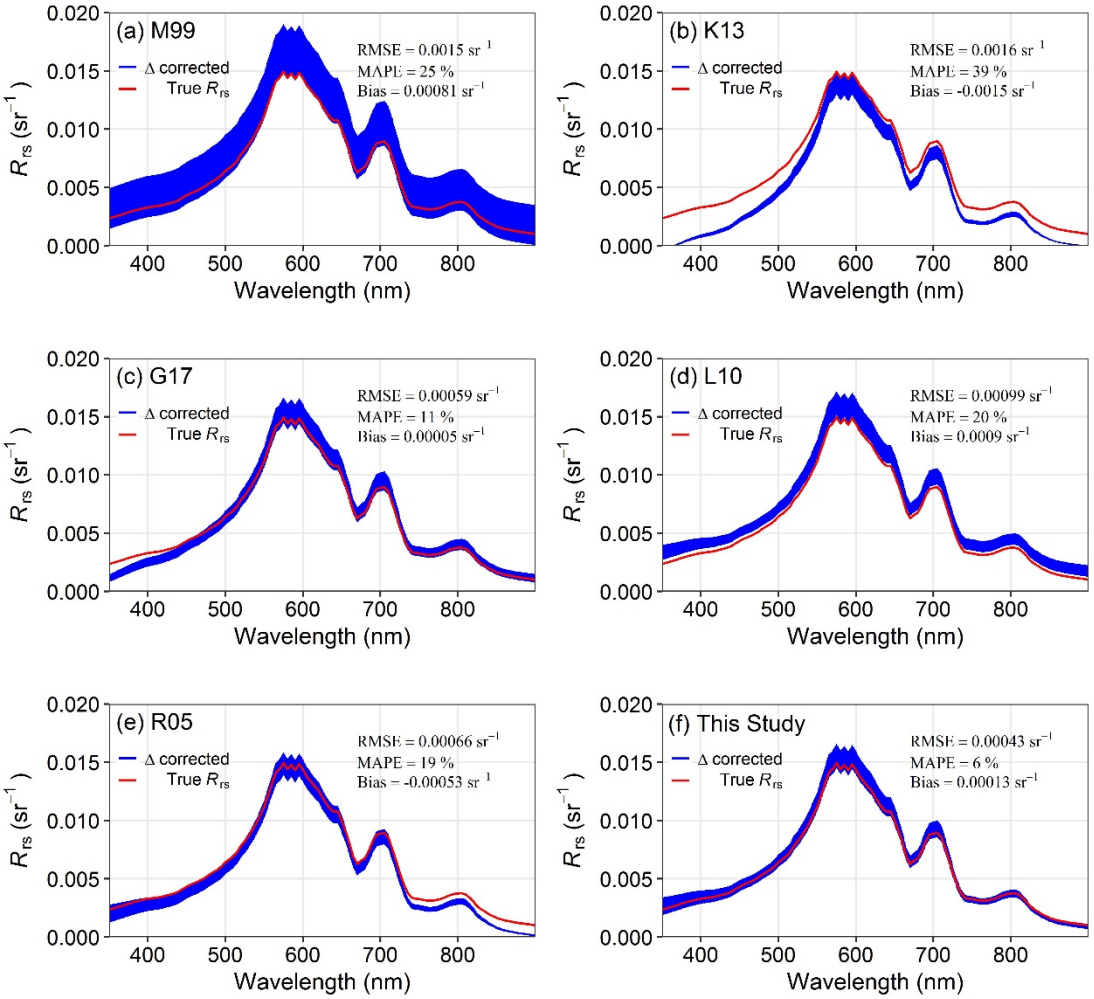

339 Fig. 7. Comparison of Δ-corrected R_{rs} spectra (blue lines) and the true R_{rs} spectrum (red line) using
340 Synthetic Dataset II. (a) R_{rs} spectra calculated using the M99 method (without Δ correction); (b) R_{rs}
341 spectra corrected using the K13 method; (c) R_{rs} spectra corrected using the G17 method; (d) R_{rs}
342 spectra corrected using the L10 method; (e) R_{rs} spectra corrected using the R05 method; (f) R_{rs}
343 spectra corrected using the new method proposed in this study.

344

345 Figure 8 shows the comparisons of the estimated and true Δ values. The estimated Δ values
346 were obtained from Synthetic Dataset III using the method proposed in this study (Eq. (14)), the
347 L10 method, and the R05 method, respectively. From the figure, it can be seen that: (1) both the L10
348 and R05 methods properly estimated Δ in clear waters (i.e., waters with $R_{rs}(720) \leq 0.0095$ sr^{-1}), but
349 significantly overestimated Δ values in turbid waters (i.e., waters with $R_{rs}(720) > 0.0095$ sr^{-1}), with

overall MAPE=161% and MAPE=213%, respectively (Figs. 8a and 8b); (2) in contrast, the method proposed in this study estimated an accurate Δ in all water types with MAPE=5% (Fig. 8c).

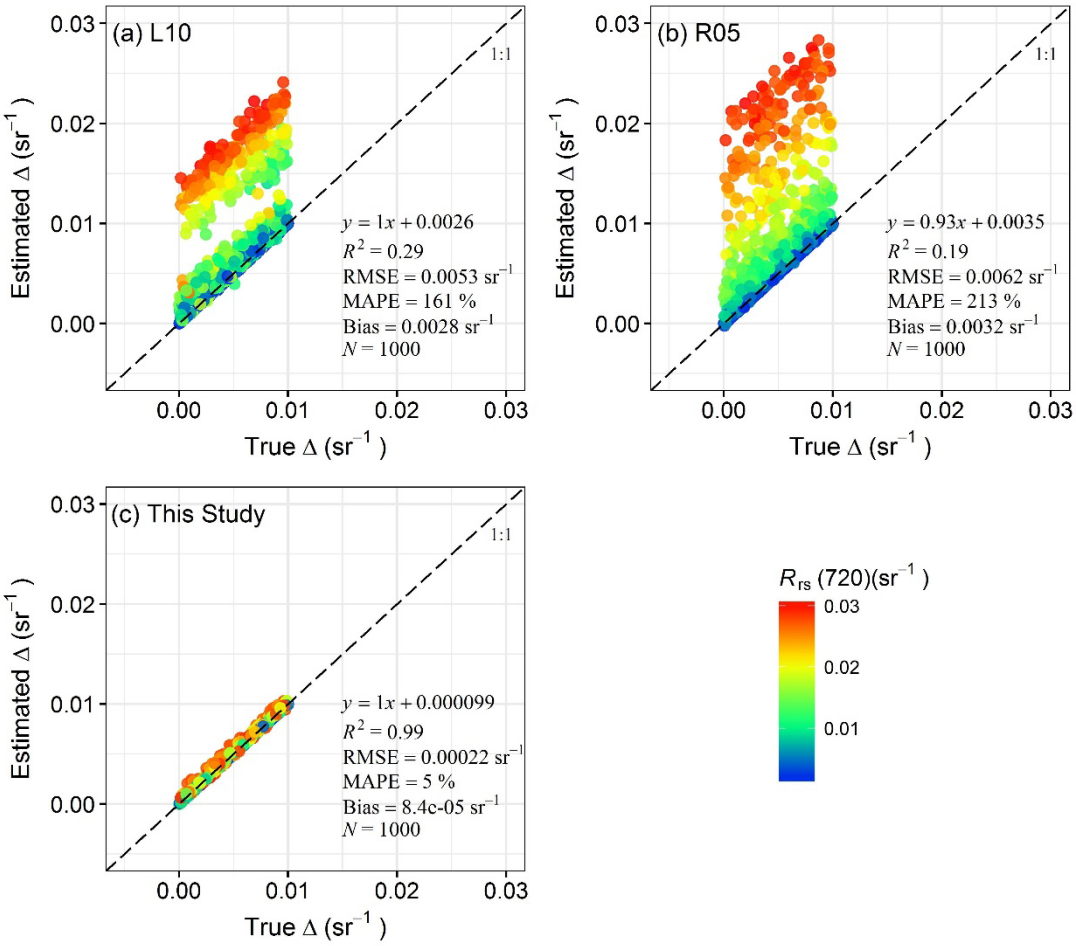

Fig. 8. Comparison of estimated and true Δ values using Synthetic Dataset III. (a) Estimated Δ values using the L10 method; (b) estimated Δ values using the R05 method; (c) estimated Δ using the method proposed in this study.

4.2 Comparison of QA scores of R_{rs} spectra before and after Δ corrections

We further compared the QA scores of the R_{rs} spectra before and after the Δ corrections for the data collected from the SeaBASS database and from Japanese inland waters, respectively (Fig. 9). For the SeaBASS data, 75% of the R_{rs} spectra had QA scores higher than 8/9 even without Δ correction because some R_{rs} spectra had already been corrected by the data providers (M99 in Fig. 9a). Nevertheless, the proportion of QA scores higher than 8/9 increased to 78% after the Δ effects

363 was corrected by the new method (this study in Fig. 9a). In contrast, the other two methods showed
364 slightly decreased quality of the R_{rs} spectra after the Δ corrections (L10 and R05 in Fig. 9a).

365 For Japanese inland waters, only 53% of the R_{rs} spectra had QA scores higher than 8/9 before
366 the Δ corrections were carried out (M99 in Fig. 9b). After the Δ corrections were carried out using
367 the new method, the proportion of QA scores higher than 8/9 increased to 66%, and the proportion
368 of R_{rs} spectra with lower QA scores decreased greatly (this study in Fig. 9b). The other Δ correction
369 methods (except for K13) also improved the quality of the R_{rs} spectra, but not as much as the new
370 method (G17, L10, and R05 in Fig. 9b).

371

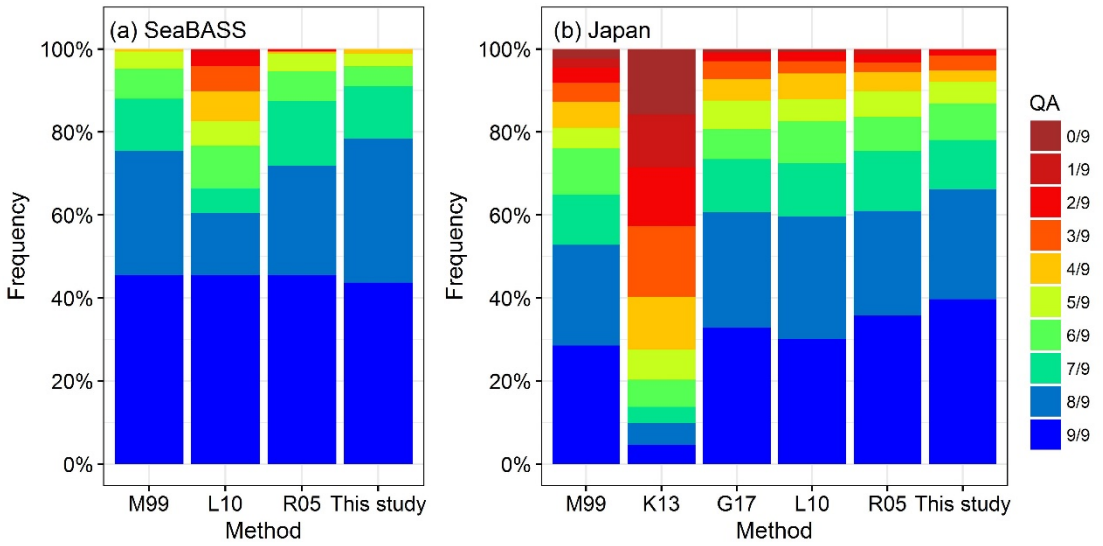

373 Fig. 9. Comparisons of QA scores of R_{rs} spectra before (M99) and after (K13, G17, L10, R05, and
374 the new method proposed in this study) Δ corrections. (a) Using R_{rs} spectra collected from the
375 SeaBASS database (N=167); (b) using R_{rs} spectra collected from 21 Japanese inland waters (N=305).

376

377 We also separated the R_{rs} spectra collected from 21 Japanese inland waters into different sky
378 condition groups using the method proposed by Groetsch et al. (2017) and compared their QA scores
379 before and after the Δ corrections for each group (Fig. 10). For the clear sky group (241 R_{rs} spectra),
380 59% of the R_{rs} spectra had QA scores higher than 8/9 before the Δ corrections were carried out, and

the proportion was increased to 69%, 65%, 61%, and 61% by the new method, R05 method, G17 method, and L10 method, respectively. The K13 method reduced the QA scores even compared to the M99 method (i.e., without Δ corrections) because CDOM-rich samples were lacking in this study (top panel in Fig. 10).

For the scattered cloud (43 R_{rs} spectra) and overcast (21 R_{rs} spectra) sky groups, the Δ correction methods greatly improved the R_{rs} spectra quality (middle and bottom panels in Fig. 10). For example, only 35% and 24% of R_{rs} spectra had QA scores higher than 8/9 in the scattered cloud and overcast sky condition groups, respectively, before Δ corrections were carried out, and the proportions increased to 56% and 57% after the Δ corrections were carried out using the new method. In particular, under the overcast sky condition, there were no R_{rs} spectra with QA scores smaller than 4/9 after the Δ corrections were made using the new method (bottom panels in Fig. 10). Except for the K13 method, the other Δ correction methods also certainly improved the R_{rs} spectra quality, with proportions of R_{rs} spectra with QA scores higher than 8/9 of 56% (scattered cloud) and 57% (overcast) for the L10 method, 56% (scattered cloud) and 62% (overcast) for the G17 method, and 47% (scattered cloud) and 48% (overcast) for the R05 method.

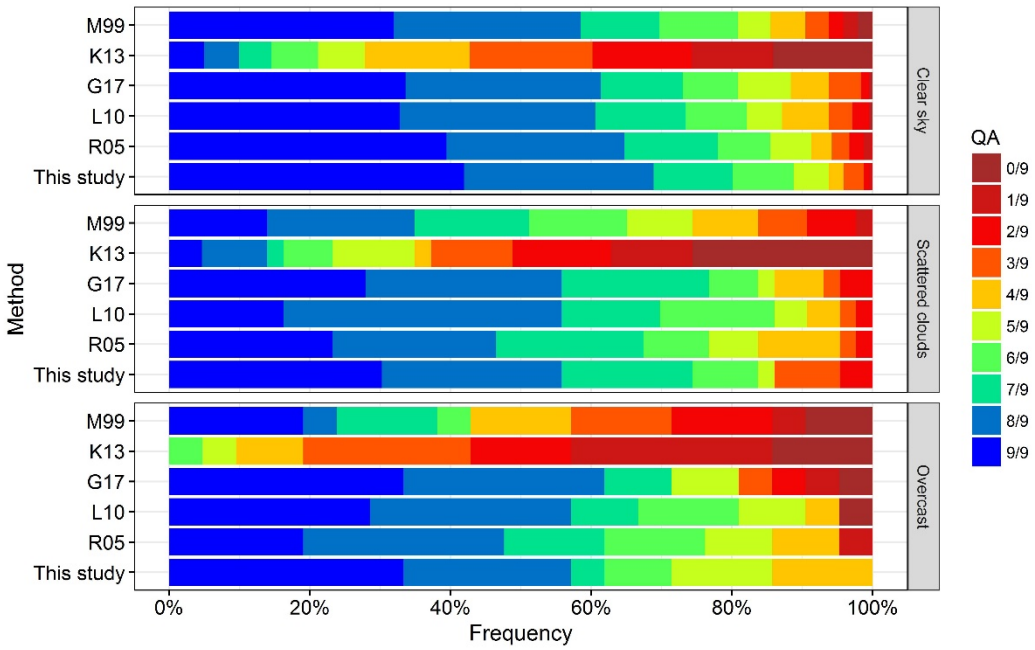

398 Fig. 10. Comparison of QA scores of R_{rs} spectra before (M99) and after (K13, G17, L10, R05, and
399 the new method proposed in this study) Δ corrections under different sky conditions. Top: under a
400 clear sky condition; middle: under a scattered clouds condition; bottom: under an overcast sky
401 condition.
402
403 4.3 Showcases for using R_{rs} spectra corrected by the new method
404 Two showcases were provided to show the usefulness of the proposed method. First we
405 compared accuracies of Z_{SD} estimations between using R_{rs} spectra before and after Δ corrections. A
406 semi-analytical algorithm developed by Jiang et al. (2019) was used to estimate Z_{SD} values from R_{rs}
407 spectra with or without Δ corrections. Figure 11 shows the comparison results. In total, 472 pairs of
408 in situ-measured R_{rs} spectra and corresponding in situ-measured Z_{SD} values, which were collected
409 from 21 Japanese inland waters and the SeaBASS database, were used. From the figure, it is not
410 surprising that the use of M99-based R_{rs} spectra (i.e., without Δ corrections) led to large errors in
411 Z_{SD} estimations with RMSE=2.5 m and MAPE=51% (Fig. 11a). In contrast, the Z_{SD} estimations
412 using R_{rs} spectra corrected by the method proposed in this study showed improved results with
413 RMSE=1.7 m and MAPE=33% as well as increased determination coefficient (0.86 vs. 0.71; Fig.
414 11b). It should be noted that there is slightly fewer data in Fig. 11a (N=469). This is because three
415 R_{rs} spectra were overcorrected, which resulted in very large Z_{SD} values (> 200 m). Those Z_{SD} values
416 were treated as outliers and not included in the results.

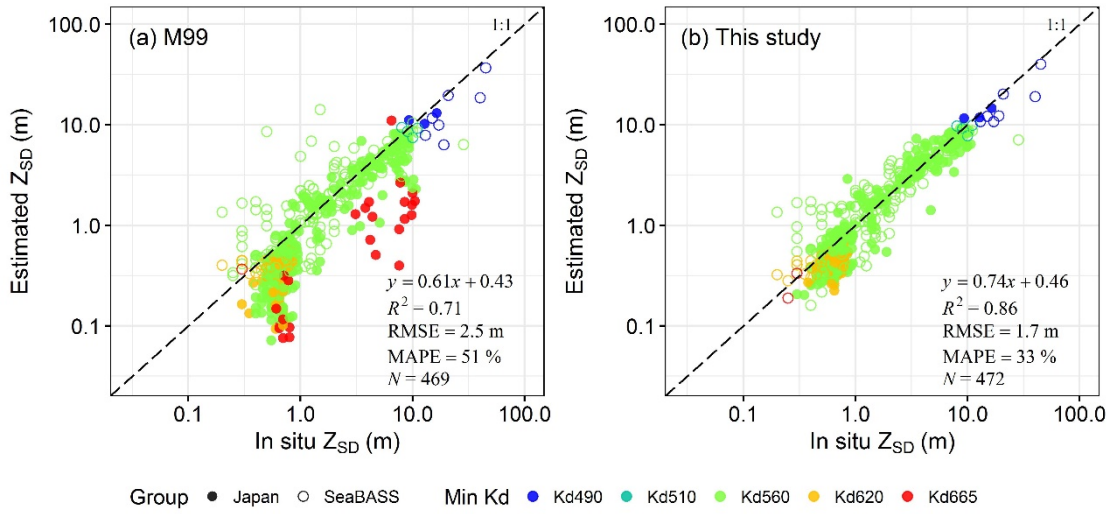

Fig. 11. Comparison of estimated and in situ-measured Z_{SD} values. The colors represent the wavelengths used for Z_{SD} estimations. (a) Estimated Z_{SD} from the M99 corrected R_{rs} spectra, which contain the residual reflected skylight; (b) estimated Z_{SD} from the R_{rs} spectra corrected by the new method proposed in this study.

Second, we compared accuracies of atmospheric correction between using R_{rs} spectra before and after Δ corrections (Fig. 12). Atmospheric corrections for three MERIS images over Lake Kasumigaura, Japan were carried out using the Case-II Processor in BEAM 5.0 (Brockmann Consult Geesthacht, Germany). The results showed that: (1) obvious overcorrections of atmospheric effects were found when the in situ R_{rs} spectra without Δ corrections were used (RMSE=0.0043 sr^{-1}, MAPE=40%, and Bias=-0.0035 sr^{-1}, Fig. 12a); (2) these overcorrections became smaller if we used in situ R_{rs} spectra with Δ corrections for comparison (RMSE=0.0032 sr^{-1}, MAPE=33%, and Bias=-0.0022 sr^{-1}, Fig. 12b). It is considered that conclusion for accuracy of atmospheric correction strongly depends on how accurate in situ R_{rs} spectra were used.

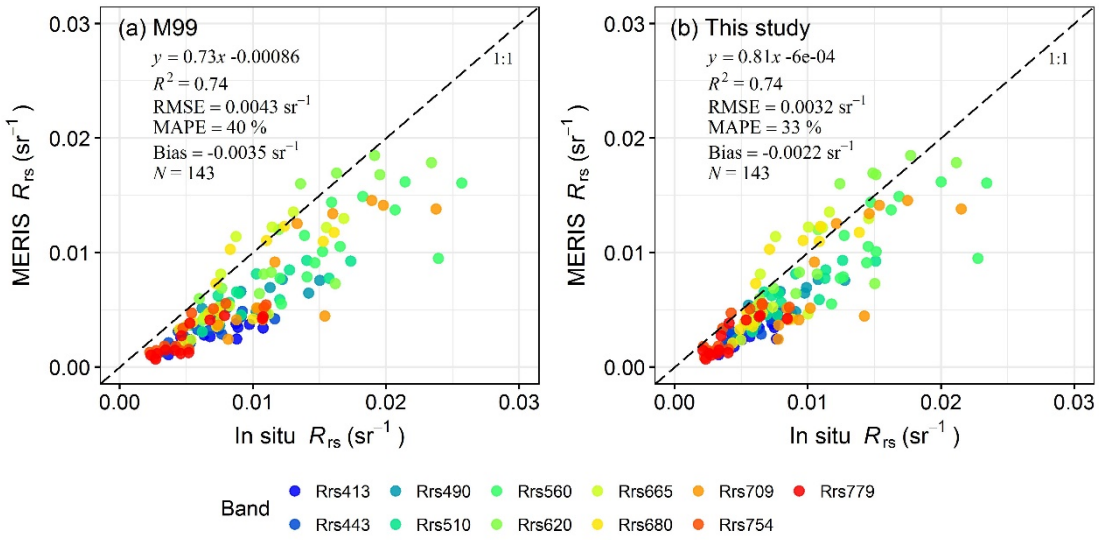

433 Fig. 12. Comparison of MERIS-derived R_{rs} and in situ-measured R_{rs} in Lake Kasumigaura, Japan.
434 (a) Using in situ R_{rs} spectra without Δ corrections; (b) using in situ R_{rs} spectra corrected by the new
435 method proposed in this study.

436

437 ## 5 Discussion

438 ### 5.1 Applicability of the proposed method

439 In this study, we proposed a new method for estimating Δ effects, which are always contained
440 in R_{rs} spectra measured in a field survey using the above-water approach (Ruddick et al., 2005; Lee
441 et al., 2010; Kutser et al., 2013; Groetsch et al., 2017). The key point of the new method is to
442 construct a relationship between RHW and Δ-free $R_{rs}(810)$ using a synthetic dataset. There are two
443 advantages for using this relationship. First, users do not need to consider Δ effects when they apply
444 the relationship. This is because the RHW is used as an independent variable in the relationship.
445 The RHW is a kind of baseline-based index, which can cancel noise coming from the environment
446 such as Δ effects or errors due to imperfect atmospheric correction (Gower et al., 1980; 2005; Hu,
447 2009; Hu et al., 2012; Matsushita et al., 2016). Therefore, we can obtain almost the same RHW
448 values even using R_{rs} spectra before Δ corrections (e.g., R_{rs} spectra from Eq. (1)). The first advantage
449 can be directly confirmed from the results in Figs. 6f, 7f and 8c, which indicate that the new method

can retrieve accurate Δ values from contaminated R_{rs} spectra (i.e., R_{rs} spectra with Δ effects).

The second advantage is that the relationship can be applied to various waters without requiring any recalibration. This is mainly because we selected three near-infrared wavelengths to calculate RHW. It has been widely known that SIOPs in the near-infrared domain are dominant only because of the absorption coefficient of pure water (Babin and Stramski, 2002; Ruddick et al., 2006; Babin et al., 2003). Therefore, it can be considered that the constructed relationship can be applied to other waters even though we only used SIOPs of Lake Kasumigaura, Japan to generate the synthetic dataset for calibrating Eq. (14). In addition, we set wide ranges of concentrations of Chl-a (0.01-300 mg/m^3) and tripton (0.01-300 g/m^3) and set the CDOM absorption coefficient at 440 nm (0.01-10 m^{-1}). These simulation ranges can cover most of the water types in the world (Moore et al., 2014).

The second advantage can be confirmed from the results shown in Fig. 7f, as we just used the default SIOPs provided by Hydrolight, which are totally different from the SIOPs used for obtaining Eq. (14). In addition, the results shown in Fig. 6f can also confirmed the proposed method does not depend on the used SIOPs because the SIOPs of Lake Chuzenji and Lake Tamblingan are probably different from those of Lake Kasumigaura. This advantage overcame the shortcomings of L10 and G17, which require SIOPs to model an R_{rs} spectrum for optimization procedure (Figs. 6c, 6d, 7c, and 7d).

In addition, the use of a non-linear relationship can overcome the shortcomings of R05, which failed in extreme turbid water ($R_{rs}(720) > 0.0095$ sr^{-1}) due to the fact that saturation effects on the R_{rs} spectra induce a ratio of $R_{rs}(720)/R_{rs}(780)$ much smaller than the constant ratio of 2.35 used in Ruddick et al. (2005). For example, the ratios of $R_{rs}(720)/R_{rs}(780)$ in Synthetic Datasets II and III varied from 1.99 to 2.03 (average of 2.01) and from 1.18 to 3.11 (average of 2.15), respectively.

5.2 Assumption of a spectral independent for Δ

In the present study, we assumed that Δ is a spectral independent parameter because its spectral

475 shape is complicated and there is still no clear theory to describe this spectral variation (Lee et al.,
476 2010). In addition, Craig et al. (2006) reported that uncertainties in R_{rs} spectra almost all come from
477 changed amplitudes of the spectra rather than changed spectral shapes. However, Groetsch et al.
478 (2017) reported that the Δ effect should be a spectrally dependent parameter. Nevertheless, their
479 results showed that the spectral shapes of water surface-reflected skylight ($\rho \cdot L_s/E_d$) are almost flat
480 under scattered clouds and overcast sky conditions, but change substantially at shorter wavelengths
481 (350–450 nm) under clear sky conditions (Fig. 5 in Groetsch et al., 2017). It should be noted that
482 the wavelength dependence of $\rho \cdot L_s/E_d$ has been partly addressed in Eq. (1), and thus the spectral
483 variation of the remaining part (Δ effects) can be considered to be small and negligible. Therefore,
484 assuming a spectrally independent Δ is probably reasonable.

485 The validity of assuming spectral independence for Δ effects can also be confirmed by our
486 results. For example, the simulation results shown in Fig. 7f and the comparison results shown in
487 Fig. 11 all indicate that the assumption is probably reasonable. From Fig. 11, it can be seen that five
488 wavelengths ranging from 490 nm to 665 nm were automatically selected for the Z_{SD} estimations in
489 different waters (Lee et al., 2015b). The Z_{SD} values estimated using different wavelengths all showed
490 acceptable estimation accuracies, which indicates that the new method can provide reasonable R_{rs}
491 spectra not only in terms of their values but also with respect to their shapes (at least in the
492 wavelength range from 490 nm to 665 nm). Nevertheless, care should be taken when using an R_{rs}
493 spectrum at a wavelength shorter than 450 nm because the inconsistencies were sometimes found
494 at these shorter wavelengths (red lines and blue lines in Fig. 6f).

495

496 5.3 Significances of Δ correction

497 In situ R_{rs} spectra are very important for the development of water quality-retrieval algorithms
498 and the evaluation of atmospheric-correction algorithms. Water quality-retrieval algorithms
499 developed based on inaccurate in situ R_{rs} spectra (e.g., containing Δ effects) will lead to erroneous

model coefficients and will have limited applicability (Kutser et al., 2013; Wei et al., 2016; Zibordi et al., 2012; also Fig. 11 in this study). In addition, atmospheric correction is a key procedure for ocean color remote sensing, and in situ R_{rs} spectra are usually used to evaluate the performance of an atmospheric correction algorithm. Using inaccurate in situ R_{rs} spectra for the evaluation might influence our judgment and thus lead to an incorrect conclusion (e.g., Fig. 12).

The results shown in Fig. 7 and Fig. 10 indicate another significant advantage of Δ correction. From the figures, it can be seen that the proposed method can correct R_{rs} spectra collected under all sky conditions and improve their quality. This finding indicates that in situ R_{rs} spectra will become usable even if they are collected under scattered clouds or overcast sky conditions. This property will relax the restriction that in situ spectrum measurement should be carried out under a clear sky, and thus can increase the number of usable in situ R_{rs} spectra in the future. Moreover, wind speed data, which are often not available in field surveys, will not be necessary to estimate a more appropriate ρ value in Eq. (1).

6 Conclusions

In this study, we proposed a new method of removing the residual reflected skylight (i.e., Δ corrections) in above-water remote sensing reflectance measurements. The proposed method is simple, effective, and universally applicable without requiring any recalibration. It can correct an in situ R_{rs} spectrum measured under various sky conditions (clear, scattered clouds, or overcast). We strongly recommend that the Δ corrections be carried out for all R_{rs} spectra measured using the above-water approach before they are applied to the development of water quality algorithms or the evaluation of atmospheric correction algorithms.

Acknowledgement:

This research was supported in part by the Grants-in-Aid for Scientific Research of MEXT

525 from Japan (No. 17H01850 and No. 17H04475A), and Kurita Water and Environment Foundation
526 Grant (18B048). We thank the European Space Agency (ESA) for providing MERIS satellite data.
527 We would also like to thank two anonymous reviewers for their valuable comments and suggestions
528 for improving the quality of the manuscript.

529

530 Reference:

531

532 Aas, E., Høkedal, J., & Sørensen, K. (2014). Secchi depth in the Oslofjord-Skagerrak area: theory,
533 experiments and relationships to other quantities. Ocean Science, 10, 177-199.
534 Babin, M., & Stramski, D. (2002). Light absorption by aquatic particles in the near-infrared spectral
535 region. Limnology and Oceanography, 47(3), 911-915.
536 Babin, M., Morel, A., Fournier-Sicre, V., Fell, F., & Stramski, D. (2003). Light scattering properties
537 of marine particles in coastal and open ocean waters as related to the particle mass
538 concentration. Limnology and Oceanography, 48(2), 843-859.
539 Bernardo, N., Alcântara, E., Watanabe, F., Rodrigues, T., Carmo, A., Gomes, A., & Andrade, C.
540 (2018). Glint removal assessment to estimate the remote sensing reflectance in inland waters
541 with widely differing optical properties. Remote Sensing, 10(10), 1655.
542 Brewin, R. J., Dall'Olmo, G., Pardo, S., van Dongen-Vogels, V., & Boss, E. S. (2016). Underway
543 spectrophotometry along the Atlantic Meridional Transect reveals high performance in satellite
544 chlorophyll retrievals. Remote sensing of environment, 183, 82-97.
545 Cai, L., Tang, D., & Li, C. (2015). An investigation of spatial variation of suspended sediment
546 concentration induced by a bay bridge based on Landsat TM and OLI data. Advances in Space
547 Research, 56(2), 293-303.
548 Cao, F., Tzortziou, M., Hu, C., Mannino, A., Fichot, C. G., Del Vecchio, R., ... & Novak, M. (2018).
549 Remote sensing retrievals of colored dissolved organic matter and dissolved organic carbon

550 dynamics in North American estuaries and their margins. Remote sensing of environment, 205,
551 151-165.
552 Choi, J. K., Park, Y. J., Ahn, J. H., Lim, H. S., Eom, J., & Ryu, J. H. (2012). GOCI, the world's first
553 geostationary ocean color observation satellite, for the monitoring of temporal variability in
554 coastal water turbidity. Journal of Geophysical Research: Oceans, 117(C9).
555 Choi, J. K., Park, Y. J., Lee, B. R., Eom, J., Moon, J. E., & Ryu, J. H. (2014). Application of the
556 Geostationary Ocean Color Imager (GOCI) to mapping the temporal dynamics of coastal water
557 turbidity. Remote Sensing of Environment, 146, 24-35.
558 Craig, S. E., Lohrenz, S. E., Lee, Z., Mahoney, K. L., Kirkpatrick, G. J., Schofield, O. M., & Steward,
559 R. G. (2006). Use of hyperspectral remote sensing reflectance for detection and assessment of
560 the harmful alga, Karenia brevis. Applied Optics, 45(21), 5414-5425.
561 Dev, P. J., & Shanmugam, P. (2014). A new theory and its application to remove the effect of surface-
562 reflected light in above-surface radiance data from clear and turbid waters. Journal of
563 Quantitative Spectroscopy and Radiative Transfer, 142, 75-92.
564 Dierssen, H. M., Kudela, R. M., Ryan, J. P., & Zimmerman, R. C. (2006). Red and black tides:
565 Quantitative analysis of water‐leaving radiance and perceived color for phytoplankton,
566 colored dissolved organic matter, and suspended sediments. Limnology and Oceanography,
567 51(6), 2646-2659.
568 Froidefond, J. M., Gardel, L., Guiral, D., Parra, M., & Ternon, J. F. (2002). Spectral remote sensing
569 reflectances of coastal waters in French Guiana under the Amazon influence. Remote Sensing
570 of Environment, 80(2), 225-232.
571 Gordon, H. R., Brown, O. B., Evans, R. H., Brown, J. W., Smith, R. C., Baker, K. S., & Clark, D.
572 K. (1988). A semianalytic radiance model of ocean color. Journal of Geophysical Research:
573 Atmospheres, 93(D9), 10909-10924.
574 Gower, J. F. R. (1980). Observations of in situ fluorescence of chlorophyll-a in Saanich Inlet.

575 Boundary-Layer Meteorology, 18(3), 235-245.
576 Gower, J., King, S., Borstad, G., & Brown, L. (2005). Detection of intense plankton blooms using
577 the 709 nm band of the MERIS imaging spectrometer. International Journal of Remote Sensing,
578 26(9), 2005-2012.
579 Goyens, C., Jamet, C., & Schroeder, T. (2013). Evaluation of four atmospheric correction algorithms
580 for MODIS-Aqua images over contrasted coastal waters. Remote Sensing of Environment, 131,
581 63-75.
582 Groetsch, P. M., Gege, P., Simis, S. G., Eleveld, M. A., & Peters, S. W. (2017). Validation of a
583 spectral correction procedure for sun and sky reflections in above-water reflectance
584 measurements. Optics express, 25(16), A742-A761.
585 Guanter, L., Ruiz-Verdú, A., Odermatt, D., Giardino, C., Simis, S., Estellés, V., ... & Moreno, J.
586 (2010). Atmospheric correction of ENVISAT/MERIS data over inland waters: Validation for
587 European lakes. Remote Sensing of Environment, 114(3), 467-480.
588 Hu, C. (2009). A novel ocean color index to detect floating algae in the global oceans. Remote
589 Sensing of Environment, 113(10), 2118-2129.
590 Hu, C., Lee, Z., & Franz, B. (2012). Chlorophyll a algorithms for oligotrophic oceans: A novel
591 approach based on three‐band reflectance difference. Journal of Geophysical Research:
592 Oceans, 117(C1).
593 Jaelani, L. M., Matsushita, B., Yang, W., & Fukushima, T. (2013). Evaluation of four MERIS
594 atmospheric correction algorithms in Lake Kasumigaura, Japan. International Journal of
595 Remote Sensing, 34(24), 8967-8985.
596 Jiang, D., Matsushita, B., Setiawan, F., & Vundo, A. (2019). An improved algorithm for estimating
597 the Secchi disk depth from remote sensing data based on the new underwater visibility theory.
598 ISPRS Journal of Photogrammetry and Remote Sensing, 152, 13-23.
599 Kirk, J. T. (2011). Light and photosynthesis in aquatic ecosystems. Cambridge University Press.

600 Knaeps, E., Dogliotti, A. I., Raymaekers, D., Ruddick, K., & Sterckx, S. (2012). In situ evidence of
601 non-zero reflectance in the OLCI 1020 nm band for a turbid estuary. Remote Sensing of
602 Environment, 120, 133-144.
603 Kou, L., Labrie, D., & Chylek, P. (1993). Refractive indices of water and ice in the 0.65- to 2.5-μm
604 spectral range. Applied optics, 32(19), 3531-3540.
605 Kutser, T., Vahtmäe, E., Paavel, B., & Kauer, T. (2013). Removing glint effects from field radiometry
606 data measured in optically complex coastal and inland waters. Remote Sensing of Environment,
607 133, 85-89.
608 Lee, Z., Ahn, Y. H., Mobley, C., & Arnone, R. (2010). Removal of surface-reflected light for the
609 measurement of remote-sensing reflectance from an above-surface platform. Optics Express,
610 18(25), 26313-26324.
611 Lee, Z., Carder, K. L., & Arnone, R. A. (2002). Deriving inherent optical properties from water
612 color: a multiband quasi-analytical algorithm for optically deep waters. Applied optics, 41(27),
613 5755-5772.
614 Lee, Z., Shang, S., Hu, C., Du, K., Weidemann, A., Hou, W., ... & Lin, G. (2015b). Secchi disk depth:
615 A new theory and mechanistic model for underwater visibility. Remote sensing of environment,
616 169, 139-149.
617 Lee, Z., Wei, J., Voss, K., Lewis, M., Bricaud, A., & Huot, Y. (2015a). Hyperspectral absorption
618 coefficient of “pure” seawater in the range of 350–550 nm inverted from remote sensing
619 reflectance. Applied Optics, 54(3), 546-558.
620 Matsushita, B., Yang, W., Jaelani, L. M., Setiawan, F., & Fukushima, T. (2016). Monitoring Water
621 Quality with Remote Sensing Image Data. Remote Sensing for Sustainability; CRC Press:
622 Boca Raton, FL, USA, 163-189.
623 Mueller, J. L., Davis, C., Arnone, R., Frouin, R., Carder, K., Lee, Z. P., ... & McLean, S. (2000).
624 Above-water radiance and remote sensing reflectance measurements and analysis protocols.

625 Ocean Optics protocols for satellite ocean color sensor validation Revision, 2, 98-107.
626 Mobley, C. D. (1994). Light and water: radiative transfer in natural waters. Academic press.
627 Mobley, C. D. (1999). Estimation of the remote-sensing reflectance from above-surface
628 measurements. Applied optics, 38(36), 7442-7455.
629 Moore, T. S., Dowell, M. D., Bradt, S., & Verdu, A. R. (2014). An optical water type framework for
630 selecting and blending retrievals from bio-optical algorithms in lakes and coastal waters.
631 Remote sensing of environment, 143, 97-111.
632 Nechad, B., Ruddick, K. G., & Park, Y. (2010). Calibration and validation of a generic multisensor
633 algorithm for mapping of total suspended matter in turbid waters. Remote Sensing of
634 Environment, 114(4), 854-866.
635 Pope, R. M., & Fry, E. S. (1997). Absorption spectrum (380–700 nm) of pure water. II. Integrating
636 cavity measurements. Applied optics, 36(33), 8710-8723.
637 Qiu, Z. (2013). A simple optical model to estimate suspended particulate matter in Yellow River
638 Estuary. Optics Express, 21(23), 27891-27904.
639 Ruddick, K. G., De Cauwer, V., Park, Y. J., & Moore, G. (2006). Seaborne measurements of near
640 infrared water‐leaving reflectance: The similarity spectrum for turbid waters. Limnology and
641 Oceanography, 51(2), 1167-1179.
642 Ruddick, K., De Cauwer, V., & Van Mol, B. (2005). Use of the near infrared similarity reflectance
643 spectrum for the quality control of remote sensing data. Remote Sensing of the Coastal Oceanic
644 Environment. International Society for Optics and Photonics.
645 Song, K., Li, L., Tedesco, L. P., Li, S., Clercin, N. A., Hall, B. E., ... & Shi, K. (2012). Hyperspectral
646 determination of eutrophication for a water supply source via genetic algorithm–partial least
647 squares (GA–PLS) modeling. Science of the Total Environment, 426, 220-232.
648 Vahtmäe, E., Kutser, T., Martin, G., & Kotta, J. (2006). Feasibility of hyperspectral remote sensing
649 for mapping benthic macroalgal cover in turbid coastal waters—a Baltic Sea case study.

Remote Sensing of Environment, 101(3), 342-351.

Wang, M., Son, S., & Shi, W. (2009). Evaluation of MODIS SWIR and NIR-SWIR atmospheric correction algorithms using SeaBASS data. Remote Sensing of Environment, 113(3), 635-644.

Wei, J., Lee, Z., & Shang, S. (2016). A system to measure the data quality of spectral remote‐sensing reflectance of aquatic environments. Journal of Geophysical Research: Oceans, 121(11), 8189-8207.

Wernand, M. R. (2010). On the history of the Secchi disc. Journal of the European Optical Society-Rapid Publications, 5.

Yang, W., Matsushita, B., Chen, J., & Fukushima, T. (2011). Estimating constituent concentrations in case II waters from MERIS satellite data by semi-analytical model optimizing and look-up tables. Remote sensing of environment, 115(5), 1247-1259.

Zhang, M., Tang, J., Dong, Q., Song, Q., & Ding, J. (2010). Retrieval of total suspended matter concentration in the Yellow and East China Seas from MODIS imagery. Remote Sensing of Environment, 114(2), 392-403.

Zhang, X., Hu, L., & He, M. X. (2009). Scattering by pure seawater: effect of salinity. Optics Express, 17(7), 5698-5710.

Zibordi, G., Ruddick, K., Ansko, I., Moore, G., Kratzer, S., Icely, J., & Reinart, A. (2012). In situ determination of the remote sensing reflectance: an inter-comparison. Ocean Science, 8(4), 567-586.